Journal of
Composites Science

MDPI

Article

The Balanced Bending Stiffness Method for Characterizing Interfacial Properties of Overmolded Composites

Ali Rezaei [1,2,*], Simon Nakze [1,2], Jos. M. H. Linsen [1,2], Rick. A. C. Leuven [1,2] and A. Tessa ten Cate [1,2]

[1] The Netherlands Organization for Applied Scientific Research (TNO), High Tech Campus 25, 5656 AE Eindhoven, The Netherlands
[2] Brightlands Materials Center, Urmonderbaan 22, 6167 RD Geleen, The Netherlands
* Correspondence: ali.rezaei@tno.nl

Abstract

This study introduces the Balanced Bending Stiffness (BBS) method, a novel experimental approach to measure the intrinsic Mode-I interfacial fracture toughness (G_{IC}) in overmolded hybrid composites. Traditional testing methods for these asymmetric systems are complicated by inherent stiffness mismatches that couple opening and shearing failure modes, requiring complex post-analytical corrections. The BBS method addresses this challenge by engineering physically balanced Asymmetric Double Cantilever Beam (ADCB) specimens through comparative stiffness matching, isolating pure mode-I failure conditions and enabling direct toughness measurement. The method is validated using a glass fiber–reinforced polypropylene (GF/PP) system, with parametric studies investigating the effects of fiber content and processing temperatures on interfacial toughness for short-fiber (SFT) and long-fiber (LFT) thermoplastics. Results reveal that higher fiber content and substrate preheating significantly enhance toughness, with particularly strong results for LFTs due to fiber bridging. This work provides a framework for material characterization and insights into optimizing overmolded composite interfaces.

Keywords: overmolding; polymer composite; fiber reinforced; interface; fracture; hybrid material

1. Introduction

The injection overmolding of continuous fiber-reinforced polymer (CFRP) composites is an advanced manufacturing technology for producing lightweight, structurally integrated, and multifunctional components. Figure 1 schematically depicts the injection overmolding process sequence. By combining thermoforming of high-performance CFRP substrate with the design freedom of injection molding, this process enables cost-effective mass production of hybrid structures with consolidated parts and integrated features such as ribs and bosses. Consequently, overmolded hybrid composites are increasingly utilized in demanding sectors like automotive and aerospace, where weight reduction and component efficiency are key factors [1].

The structural integrity and overall performance of these components critically depend on the quality and robustness of the interface formed between the CFRP substrate and the overmolded thermoplastic. Figure 2 schematically illustrates the interface development in injection overmolded parts, where, after initial contact of the overmolding material with the substrate surface, material diffusion occurs and fiber migration may form.

Academic Editor: Francesco Tornabene

Received: 12 November 2025
Revised: 22 January 2026
Accepted: 2 February 2026
Published: 10 February 2026

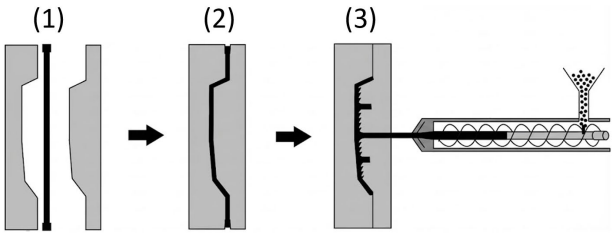

Figure 1. Schematic of the injection overmolding process sequence: (1) placement of the substrate into the mold, (2) forming of the substrate upon mold closure, and (3) injection overmolding to consolidate the final component.

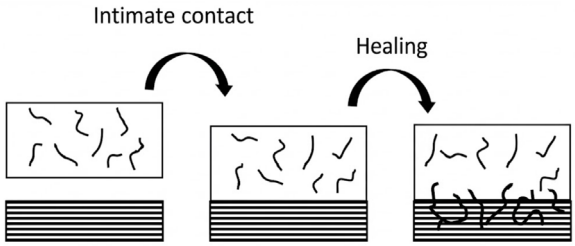

Figure 2. Simplified schematic of interface development during the injection overmolding process, describing thermoplastic polymers diffusing into the interface from the overmolding material.

Despite its industrial significance, the scientific understanding of this bimaterial interface remains underdeveloped. Although the interface is widely acknowledged as the mechanically weakest region, its characterization remains immature, and existing methods for quantifying interfacial fracture behavior are limited and often incomplete [2]. This deficiency presents a significant barrier to reliable mechanical design and failure prediction. The primary difficulty arises from the inherent hybrid and asymmetric nature of the material system, which invalidates many classical testing procedures and complicates the interpretation of experimental results [3,4].

Recent research has actively investigated the mechanical optimization of these hybrid systems, particularly regarding processing parameters and material composition. For instance, Ziaee et al. [5] demonstrated the critical role of high fiber content in enhancing the performance of thermoplastic composites, while Jiang et al. [6] highlighted the superior impact properties of long-fiber thermoplastics (LFT) compared to short-fiber counterparts. Similarly, Miao et al. [7], Yan et al. [8], and Heitkamp et al. [9] have studied the effects of injection parameters, interface crystallization, and numerical predictions on bond integrity. However, these investigations predominantly rely on component-level tests, such as single-lap shear, T-peel, or tensile pull-off configurations. While valuable for ranking structural performance, these methods inherently induce mixed-mode stress states—coupling opening (Mode-I) and shearing (Mode-II) forces and are heavily influenced by specimen geometry (e.g., rib thickness or overlap length) rather than measuring the intrinsic adhesion properties. Consequently, such approaches often fail to isolate the true interfacial fracture toughness required for accurate failure prediction, which is the gap that this study addresses via the BBS method. Moreover, in industry, T-shaped specimens and pull-out test methods are often used for understanding the behavior of overmolded materials, but these approaches are very basic and do not reveal true interfacial fracture characteristics [10].

In an overmolding interface, a stiff, anisotropic CFRP substrate is bonded to a more compliant, quasi-isotropic thermoplastic overmold, creating an inherently asymmetric system. This asymmetry violates the core assumptions of classical beam theory, leading to dissimilar bending stiffnesses in the cracked arms. A foundational theoretical framework for analyzing such bimaterial interfaces established that this mismatch in elastic properties inherently couples the opening (Mode-I) and shearing (Mode-II) failure modes at the

crack tip [4,11]. According to this framework, even under pure tensile loading, a crack at a dissimilar interface experiences a mixed-mode stress state, and interfacial toughness becomes a function of this mode-mixture.

While analytically elegant, the use of this theoretical approach presents significant practical challenges. Its application requires sophisticated data post-processing to deconstruct mixed-mode effects and yields a complex function rather than a single, discrete value for the intrinsic Mode-I toughness. This complexity hinders its use in rapid material screening or process optimization studies.

Some research has employed advanced experimental techniques like Digital Image Correlation (DIC) or numerical approaches like Cohesive Zone Modeling (CZM) to address the complex fracture behavior. While numerical methods such as Cohesive Zone Modeling (CZM) are widely established for simulating delamination, they are inherently dependent on accurate experimental inputs. Specifically, CZM requires a precise, mode-pure measurement of the critical energy release rate (G_{IC}) to define the traction-separation laws that govern crack initiation and propagation. Without reliable experimental data free from mixed-mode artifacts, these models cannot be accurately calibrated. Thus, a robust experimental framework is first required to provide these intrinsic material parameters [12–14].

This paper presents a novel experimental procedure, termed the Balanced Bending Stiffness (BBS) Method, which shifts the paradigm from post-analytical correction to a priori experimental design. Instead of accepting the specimen's asymmetry, the BBS method utilizes a comparative procedure to engineer a physically balanced specimen where symmetric crack propagation is achieved. By systematically adjusting the specimen's geometry to match the bending stiffness of the substrate and the overmolding material, this method experimentally isolates a pure Mode-I failure condition, enabling direct determination of the intrinsic Mode-I interfacial fracture toughness, G_{IC}. The balanced stiffness principle underlying this method could potentially be extended to other asymmetric test configurations, such as End-Notched Flexural (ENF) specimens for Mode-II characterization, though this study focuses specifically on the Mode-I ADCB implementation.

The research has two primary objectives: First, it introduces and validates the BBS method for measuring the true Mode-I interfacial fracture toughness of overmolded hybrid composites. Second, it applies this method to conduct a systematic parametric study on a common automotive material system of overmolded glass fiber–reinforced polypropylene composites.

2. Materials and Methods

2.1. Materials

The materials used in this study are representative of glass-fiber reinforced polypropylene (GF/PP) systems widely adopted in automotive components. The substrate plates were produced using a unidirectional (UD) GF/PP tape (BUFA® MCP1238). This tape contains 70 wt.% continuous glass fibers and has an axial tensile modulus of 40 GPa and a tensile strength of 890 MPa.

- The tape has an initial ply areal weight of 220 g/m^2 and a thickness of about 0.22 mm. After consolidation (described in Section 2.2), the average cured ply thickness was approximately 0.18 mm.

The overmolding materials comprised both short- and long-fiber reinforced thermoplastics:

- Short-Fiber Thermoplastics (SFT): Three SFT grades (SABIC® PP compounds) containing 20, 30, and 40 wt.% glass fiber were used. Their tensile strengths ranged from 80 to 110 MPa, and their tensile moduli from 4.5 to 8.9 GPa. SFT is currently the most common material industrially used for injection overmolding.

- Long-Fiber Thermoplastics (LFT): Due to their emerging use and superior mechanical performance, three LFT grades of Celstran® (PP-GF30, PP-GF40, and PP-GF50) were also studied. Their tensile strengths ranged from 120 to 170 MPa, and their tensile moduli from 7 to 10.5 GPa. The initial fiber length in these materials is 15 mm.

2.2. Specimen Fabrication and Test Configuration

Specimen preparation began with substrate panel fabrication from UD GF/PP tape. Plies were stacked based on initial balancing estimates and consolidated in a press using an optimized cycle to minimize voids and residual stress: preheating to 230 °C under minimal pressure for 3–5 min, applying 1.0–1.5 MPa at 230 °C for 5 min, cooling under pressure to 140–160 °C for 2–5 min, and final cooling to 23 °C for 10–15 min. Panels underwent visual inspection for fiber waviness, multi-point thickness checks (variation $\leq \pm 3\%$), and mass-balance verification to detect resin loss or voids, ensuring high-quality substrates.

Overmolding experiments were conducted on an ENGEL 50-ton injection molding machine equipped with a high-speed robotic transfer system and an infrared (IR) preheating station. Substrates were prepared with dimensions of 10×30 cm^2. During the process, the robot positioned the substrate in the IR oven to reach the target preheat temperature, then immediately transferred it to the mold and clamping actuators. The total transfer time from the IR oven to the start of injection was maintained at 5 s. Once the mold closed, the injection overmolding of the melt was performed via side injection approach to ensure uniform distribution over the substrate. For every injection, the substrate and melt temperatures were set according to the study target and the remaining process settings were fixed for all experiments: fill rate 55 cm^3/s, pack/hold 400 bar for 20 s, and cooling 25 s. Figure 3 illustrates the detailed components of the injection overmolding setup utilized in this study.

For Digital Image Correlation (DIC) during ADCB testing, the camera-facing side of each specimen was gently abraded (P1000) and degreased. A thin, matte white base coat was sprayed, followed by a high-contrast black speckle pattern (3–6 pixels spot size) with an approximately 45–55% coverage. All fracture toughness measurements were conducted on five specimens per condition, with injection overmolding performed on three different panels for each test configuration to ensure statistical reliability. Single-camera 2D DIC was employed to track crack propagation and rigorously verify Mode-I isolation. Images were acquired using a 12 MP camera with a fixed focal length lens, aligned normal to the specimen surface. The Field of View (FOV) was set to 60–90 mm, yielding a spatial resolution of approximately 20–30 µm/pixel. Images were recorded at 1–5 Hz and synchronized with the load–displacement data. Correlation was performed using VIC-2D v7.2 software (Correlated Solutions, Inc.). A subset size of 25–35 pixels and a step size of 5–7 pixels were selected to optimize the balance between spatial resolution and displacement noise (measured at $\leq$0.05 pixels). Green-Lagrange strains were computed using a 5–7 point decay filter. To ensure the validity of the BBS method, a strict quantitative mode-mixity criterion was applied. The near-tip displacement fields were fitted to a Williams-series expansion to extract the stress intensity factors (K_I, K_{II}) [15]. Only data points exhibiting a mode-mixity ratio of $|K_{II}/K_I| < 0.10$ were accepted for the calculation of fracture toughness (G_{IC}), confirming that the customized stiffness balancing effectively suppressed shear modes. Figure 4 presents representative DIC outputs, illustrating the strain distribution characteristic of pure Mode-I fracture.

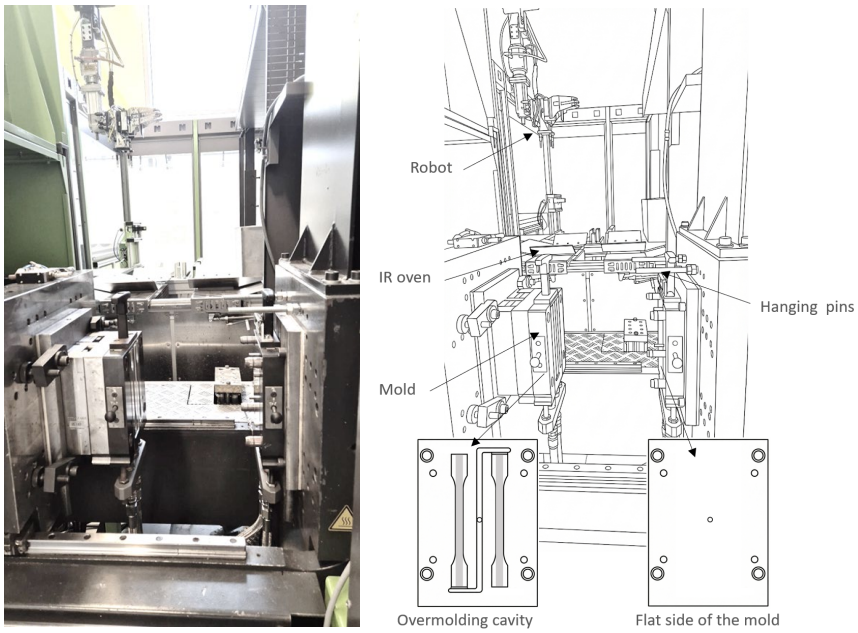

Figure 3. Detailed engineering figure and drawing of the injection overmolding station. The integrated setup consists of a robotic transfer arm, an infrared (IR) preheating oven, and the injection mold assembly equipped with hanging pins for substrate fixation. The bottom insets show the front view of the mold faces, including the overmolding cavity, designed for the production of one or two specimens per cycle. The process involves automated robotic handling of the UD substrate from the IR station to the mold, followed by side-injection of the melt to ensure uniform fiber orientation in the overmolding layer.

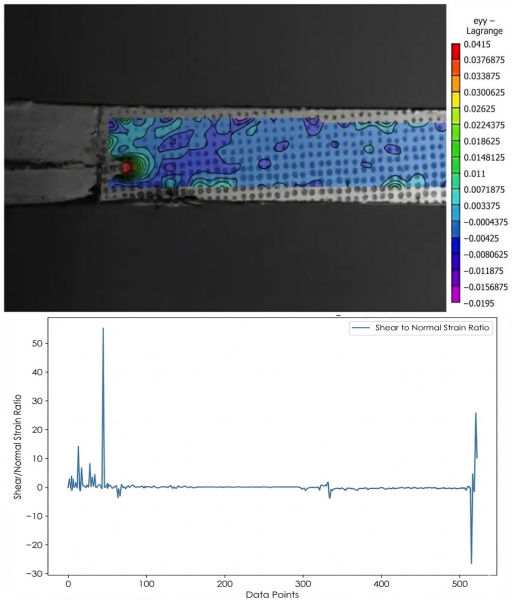

Figure 4. Mode-mixity validation using Digital Image Correlation (DIC): (**top**) Representative full-field ε_{yy} strain map showing symmetric strain concentration at the crack tip; (**bottom**) Evolution of principal strains along the crack path, confirming the dominance of Mode-I opening strains and minimal shear contribution.

Mode-I tests were performed using Instron universal testing machine with a load cell under displacement control at 3 mm/min. Specimens were mounted as shown in Figure 5, to aid side-view imaging. DIC was used to measure the crack length and verify mode purity from the strain fields of ε_{yy} and ε_{xy}. Load (P), crosshead displacement (δ),

and synchronized images were acquired continuously. Short unload–reload segments were introduced every ≈5 mm of crack advance to stabilize compliance readings.

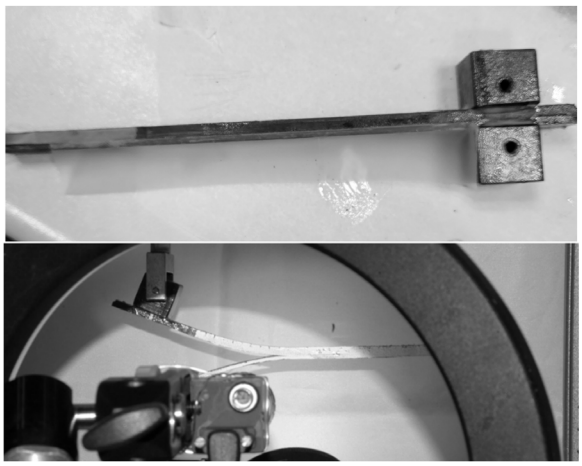

Figure 5. Experimental setup for the Asymmetric Double Cantilever Beam (ADCB) test. (**Top**) Specimen mounted in the loading blocks; (**Bottom**) Side-view camera alignment used for real-time DIC monitoring of the crack tip.

2.3. Methodology Concept

The Balanced Bending Stiffness (BBS) method addresses interfacial fracture characterization in overmolded hybrid composites by prioritizing experimental symmetry to isolate pure Mode-I conditions. Traditional approaches to measuring interfacial fracture toughness (G_{IC}) in asymmetric systems are confounded by stiffness mismatches, which couple opening (Mode-I) and shearing (Mode-II) failure modes, requiring complex post hoc corrections [16]. The BBS Method circumvents this by competitively balancing the bending stiffness of the substrate and overmolding material ($E_{sub}I_{sub} = E_{om}I_{om}$), nullifying shear contributions ($G_{II} \approx 0$) and enabling direct measurement of intrinsic Mode-I toughness through stable, interfacial crack propagation. This a priori design delivers a discrete G_{IC} value, streamlining material screening and process optimization compared to conventional methods reliant on mixed-mode deconvolution.

The method employs a systematic procedure: elastic moduli of the substrate and overmolding material are determined via tensile tests and are used to define initial specimen geometry (using $E_{sub}I_{sub} = E_{om}I_{om}$). Hybrid specimens are fabricated through overmolding, tested using an Asymmetric Double Cantilever Beam (ADCB) configuration, and if needed, refined by adjusting substrate thickness (e.g., via ply addition or removal) until symmetric crack growth along the interface confirms Mode-I isolation. This validated geometry serves as the foundation for all subsequent toughness measurements. The balanced and unbalanced ADCB configurations illustrated in Figure 6.

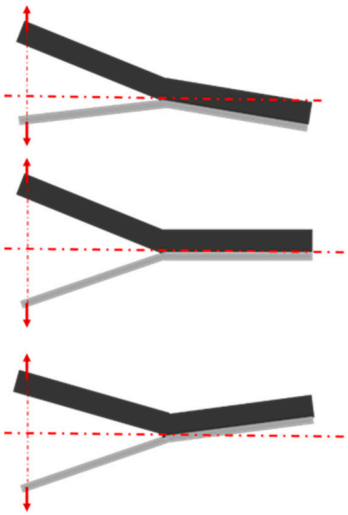

Figure 6. Schematic comparison of ADCB deformation modes: (**Top**/**Bottom**) Unbalanced stiffness configurations ($E_{sub}I_{sub} \neq E_{om}I_{om}$) leading to mixed-mode crack tip rotation; (**Center**) Balanced stiffness configuration $E_{sub}I_{sub} = E_{om}I_{om}$) resulting in symmetric Mode-I opening without shear coupling. The dashed line indicates the neutral-axis deformation path.

2.4. Fracture Toughness Calculation

After ADCB testing, interfacial fracture toughness (G_{IC}) is determined from load–displacement data using a modified Compliance Calibration Method (CCM), based on the principles in ASTM D5528 [17]. For stable crack propagation, G_{IC} is computed from the fundamental energy release rate equation:

$$G_{IC} = \frac{P^2}{2b}\frac{dC}{da} \tag{1}$$

where P is the applied load, b is the specimen width, a is the crack length, and C is the specimen compliance ($C = \delta/P$, δ is displacement).

The standard ASTM method plots $C^{1/3}$ against 'a' to find a linear fit. However, this simple beam-theory model does not fully account for non-ideal effects like fixture compliance, shear deformation, or crack root rotation, which are especially relevant in ADCB testing. To improve the physical accuracy, a dimensionless normalization factor, N, is introduced to correct for these boundary and system effects. The corrected calibration fit is:

$$\left(\frac{C}{N}\right)^{\frac{1}{3}} = m(a + \Delta) \tag{2}$$

where m is the slope and Δ is the crack length correction factor found from the x-axis intercept of the linear fit. Differentiating the compliance with respect to crack length a (assuming N is a constant for the system) yields the derivative:

$$\frac{dC}{da} = 3Nm^3(a + \Delta)^2 \tag{3}$$

Substituting Equation (3) back into the fundamental energy equation (Equation (1)) gives the equation for the corrected Compliance Calibration Method, which is used for all G_{IC} calculations from stable crack growth:

$$G_{CCM}(a) = \frac{3NP^2m^3(a + \Delta)^2}{2b} \tag{4}$$

In cases of unstable, stick-slip crack propagation characterized by load build-up and sudden drops, the Area Method (energy balance) is employed:

$$G_{IC} = \frac{\int P d\delta}{b\Delta a} \quad (5)$$

Here, $\int P d\delta$ represents the work done over a crack increment Δa, calculated as the area under the load–displacement curve for the corresponding crack advance. This method is robust for erratic crack growth, capturing energy release across unstable jumps.

To ensure reliability, G_{IC} values from CCM and the Area Method are cross-validated, requiring agreement within 10%. The CCM result is prioritized for stable propagation, while the Area Method is favored for stick-slip cases due to its robustness against instability. This dual approach ensures accurate and reproducible toughness measurements across diverse material behaviors. Figure 7 summarizes the schematic flowchart of the proposed BBS Method.

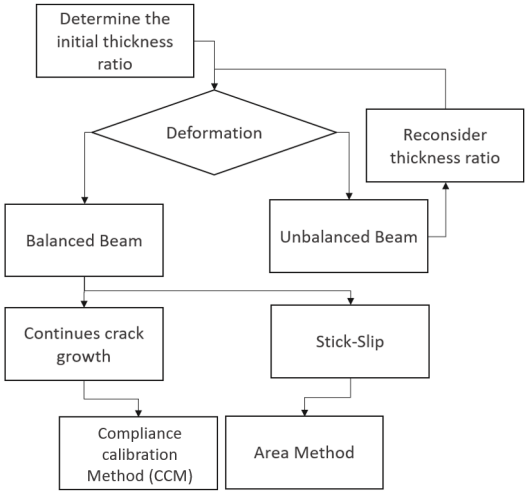

Figure 7. Schematic flowchart of the Balanced Bending Stiffness (BBS) Method.

3. Results

3.1. BBS Method Validation and Proof of Concept

To demonstrate the full methodology, the SFT30 material is used as a case study.

Following the balancing procedure $E_{sub}h_{sub}^3 = E_{om}h_{om}^3$, the required substrate thickness for the fixed 4.0 mm overmolding thickness was calculated using the material moduli 40 GPa for the substrate and 6.5 GPa for SFT30:

$$h_1 \approx h_2\left(\frac{E_2}{E_1}\right)^{\frac{1}{3}} \approx 4.0\left(\frac{6.5}{40}\right)^{\frac{1}{3}} \approx 2.18 \text{ mm}$$

This thickness corresponds to 12 UD plies. As shown in Figure 8, test coupons with 11, 12, and 13 plies were manufactured and tested. The 12-ply configuration (center) shows symmetric crack growth, validating the stiffness balance ($r = \frac{E_1 h_{1sub}^3}{E_2 h_{2OM}^3} \approx 1$) and confirming pure Mode-I conditions.

The load–displacement ($P - \delta$) curve for a balanced SFT30 specimen is shown in Figure 9. Specimen compliance was calculated at each unload segment and plotted as $(C/N)^{1/3}$ versus the DIC-measured crack length a (Figure 10) to determine the parameters m and Δ. The fracture toughness was then calculated using the corrected CCM Equation (4). For example, at a crack length a = 45.2 mm, the corresponding average load was about 42 N. Using the derived parameters (N, m, Δ) from the fit, the toughness G_{CCM} is 1.035 kJ/m^2.

This value was cross-validated using the Area Method which yielded G_{Area} = 1.008 kJ/m^2. As the corrected CCM and Area methods agreed within 3% (well within the required 10%), the values were accepted and this procedure was automated.

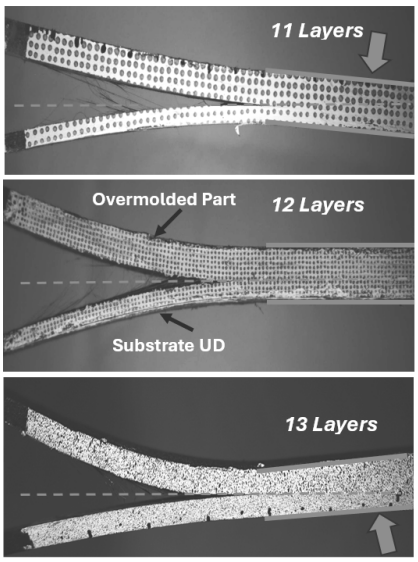

Figure 8. Balancing trial for SFT 30 overmolding material, showing (**top** to **bottom**) 11, 12, and 13-ply substrates. The 12-ply configuration (**center**) shows symmetric Mode-I crack propagation.

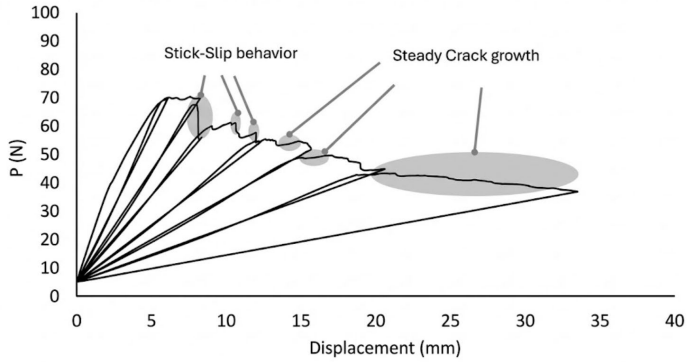

Figure 9. Representative Load–Displacement ($P - \delta$) response for SFT30 specimens (Process: T_{melt} = 230 °C, $T_{preheat}$ =120 °C). The curve illustrates regions of stable crack growth used for Compliance Calibration (CCM) versus stick-slip propagation analyzed via the Area Method.

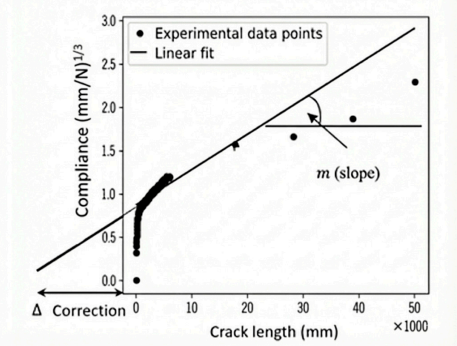

Figure 10. Normalized compliance calibration plot vs. crack length derived from experimental data. The linear regression fit is used to extract the crack length correction factor (Δ) from the x-intercept and the slope (m) for the corrected toughness calculation (Equation (4)).

3.2. Parametric Study

With the BBS method validated in Section 3.1 for isolating pure Mode-I failure, it was applied to conduct a comprehensive parametric study. This study focused on two critical variables: the weight fraction of glass fibers in the overmolding compound (20%, 30%, and 40% for SFT; 30%, 40%, and 50% for LFT) and the substrate preheating temperature (110 °C, 120 °C, and 130 °C). These variables were selected due to their significant impact on interface formation and polymer chain mobility.

As a first step, the balancing procedure was applied to all material combinations. The balancing converged within 2–3 thickness adjustments for all systems. Table 1 summarizes the final, refined substrate configurations, showing the corresponding thickness to each overmolding material.

Table 1. Injection overmolding materials and relevant substrate UD layer configuration.

Overmolding Material	Fiber Content	Tested Elastic Modulus (GPa)	Number of UD Layers in substrate	Corresponding Thickness (mm)
SFT 20	20 wt.%	4.95	11	1.99 ± 0.03
SFT 30	30 wt.%	6.5	12	2.18 ± 0.02
SFT 40	40 wt.%	8.96	14	2.43 ± 0.04
LFT 30	30 wt.%	6.58	12	2.19 ± 0.02
LFT 40	40 wt.%	8.35	13	2.37 ± 0.05
LFT 50	50 wt.%	11.6	15	2.64 ± 0.03

The application of the BBS method enabled a detailed investigation into the processing-structure-property relationships of the interface. The interfacial fracture toughness G_{IC} results for Short-Fiber Thermoplastic (SFT) systems are summarized in Figure 11. The results demonstrate a systematic evolution in performance starting with the SFT 20 wt.% grade. At this baseline fiber content, the toughness showed a modest but steady response to thermal processing, with G_{IC} rising from 0.75 kJ/m^2 at 110 °C to 0.86 kJ/m^2 at 130 °C. Increasing the reinforcement to SFT 30 wt.% elevated the overall toughness range, while maintaining a similar sensitivity to process temperature. For this grade, adequate preheating lifted the adhesion values from 0.85 kJ/m^2 to 0.98 kJ/m^2 across the same temperature window. The most profound impact, however, was observed in the SFT 40 wt.% grade. Here, the synergistic effect of high fiber loading and thermal energy was evident, with G_{IC} increasing significantly from 1.10 kJ/m^2 at 110 °C to 1.38 kJ/m^2 at 130 °C. This systematic evolution confirms that while fiber content sets the baseline mechanical potential (rising by approximately 47% from 20% to 40% fiber content at 110 °C), thermal energy is the active variable required to unlock it. Notably, the magnitude of this thermal enhancement appears to scale with fiber content. This suggests that as the substrate surface softens at higher preheating temperatures, the higher fiber volume fraction increases the probability of short fibers penetrating the interface. This likely facilitates a more extensive mechanical interlocking between the overmolded short fibers and the continuous filaments of the substrate, supplementing the polymer diffusion mechanism.

Figure 12 illustrates the results for Long-Fiber Thermoplastic (LFT) systems, which exhibit a distinct and highly responsive behavior to processing parameters. Starting with the LFT 30 wt.% grade, the data reveals a critical dependence on thermal energy to activate the adhesion mechanism. At 110 °C, the interface toughness was relatively modest (0.62 kJ/m^2). However, increasing the preheat temperature to 130 °C triggered a clear improvement, more than doubling the value to 1.32 kJ/m^2. This sharp transition suggests

that for lower LFT fractions, a thermal threshold must be crossed to ensure sufficient matrix mobility for the long fibers to effectively bridge the interface. Moving to the LFT 40 wt.% grade, the system demonstrated a more robust performance baseline. The G_{IC} values showed a strong, linear progression, climbing from 1.17 kJ/m^2 at 110 °C to 1.64 kJ/m^2 at 130 °C. Unlike the 30% grade, which required high heat to perform well, the 40% grade delivered high toughness even at intermediate temperatures, indicating a wider and more stable processing window. The highest absolute performance in this study was achieved by the LFT 50 wt.% grade. At the maximum preheating temperature of 130 °C, the interface reached a peak toughness of 1.73 kJ/m^2. Even at the lower boundary of 110 °C, this grade maintained a solid performance (1.24 kJ/m^2). These results indicate that when high fiber volume is combined with optimized thermal bonding, the long fibers create a bridging zone capable of dissipating significant energy, effectively acting as a structural reinforcement across the crack path.

Fractographic analysis provided further insights, revealing cohesive failure modes. Across all experiments, failure surfaces exhibited fibrillation, indicative of possible material penetration during overmolding. Higher preheating temperatures intensified this fibrillation, particularly in LFT systems, where more pronounced fiber pull-out and matrix deformation were observed (Figure 13). For instance, at 130 °C, LFT 40 wt.% specimens displayed extensive fibrillation compared to SFT counterparts. This cohesive failure behavior, characterized by material entanglement, likely underpins the higher toughness observed in LFTs. The BBS Method's ability to produce consistent Mode-I crack paths was essential for this analysis, enabling a clear visualization of these failure mechanisms. This highlights the method's utility in isolating and permitting the quantification of these complex toughening behaviors.

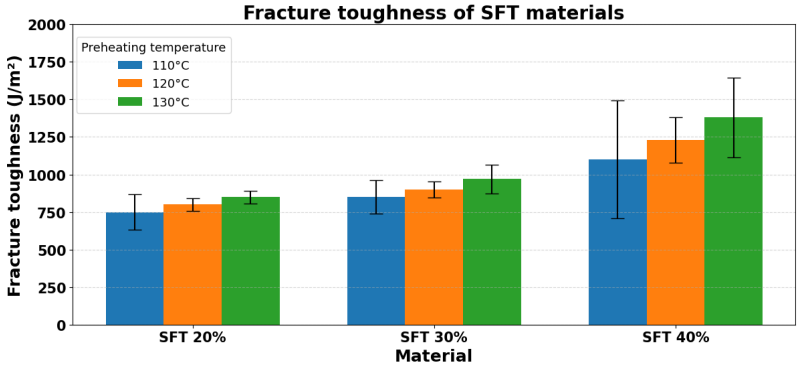

Figure 11. Effect of fiber content and substrate preheating on the interfacial toughness of SFT overmolded hybrids. The bar chart shows increase in G_{IC} driven by both higher glass fiber content (20, 30, and 40 wt.%) and elevated substrate preheating temperatures.

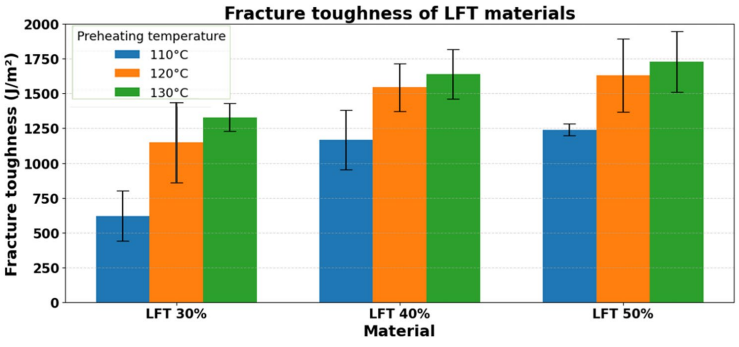

Figure 12. Effect of fiber content and substrate preheating on the interfacial toughness of LFT overmolded hybrids. The bar chart illustrates increase in G_{IC} driven by both higher glass fiber content (30, 40, and 50 wt.%) and elevated substrate preheating temperatures.

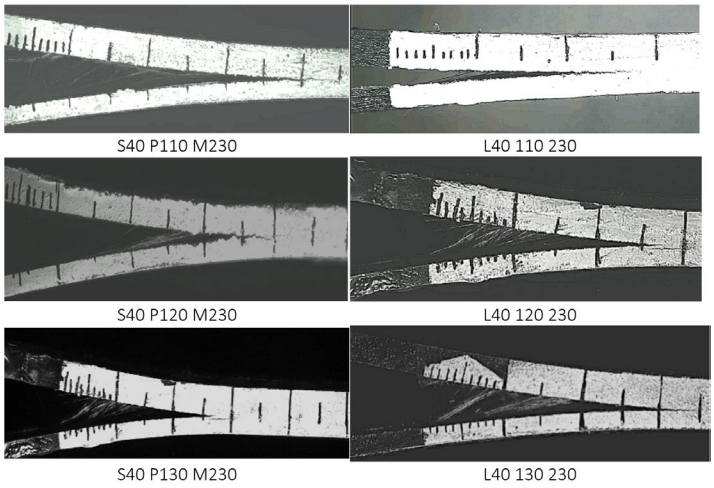

Figure 13. Micrographs of fracture surfaces for 40% fiber content specimens, comparing the limited fibrillation in Short Fiber Thermoplastics (SFT, **left**) versus extensive fiber bridging and pull-out in Long Fiber Thermoplastics (LFT, **right**), correlating with the higher G_{IC} values observed for LFTs.

A comparative assessment of the SFT and LFT results provides a broader perspective on reinforcement efficiency. Under optimal processing conditions (130 °C), the LFT systems consistently outperform their SFT counterparts. For instance, the LFT 40 wt.% grade achieved a toughness of 1.64 kJ/m^2, notably surpassing the SFT 40 wt.% grade (1.38 kJ/m^2). Interestingly, regarding reinforcement efficiency, the LFT 30 wt.% grade achieved a toughness (1.32 kJ/m^2) that is statistically comparable to the SFT 40 wt.% grade.

It must be noted that, while these comparisons strongly point to the structural advantages of the long-fiber architecture, a direct scientific correlation must be drawn with caution. As the SFT and LFT materials were commercially sourced from different suppliers, distinct differences in the base polypropylene matrix formulation and fiber sizing chemistry may contribute to the absolute adhesion values. Therefore, while fiber length appears to be a dominant factor, it cannot be strictly isolated from potential chemical variations in this specific dataset. Despite these formulation differences, the general trend is of clear importance to the industry. In this research, the LFT systems demonstrated superior performance capabilities in the overmolding process compared to the SFT grades currently dominating the market. The extensive fiber bridging observed in LFTs provides a potential mechanical reinforcement mechanism that SFTs lack.

4. Discussion

The successful application of the Balanced Bending Stiffness (BBS) method allowed for the isolation of intrinsic fracture behaviors, revealing that interfacial toughness in overmolded hybrids is governed by a competition between thermal diffusion and mechanical reinforcement. The monotonic increase in G_{IC} with substrate preheating temperature confirms the critical role of polymer chain mobility; higher interface temperatures maintain the melt above the crystallization point for longer periods, facilitating deeper interdiffusion of polymer chains across the boundary. However, the distinct performance gap between SFT and LFT indicates that matrix adhesion is not the sole contributor. The LFT systems exhibited higher toughness values compared to SFT grades under identical processing conditions. This enhancement is attributed to the fiber architecture, where longer fibers bridge the crack zone, inducing large-scale deformation and frictional pull-out. This “fiber bridging” mechanism effectively shields the crack tip, requiring higher energy input for propagation.

Quantitatively, the interfacial fracture toughness values obtained in this study are consistent with the order of magnitude reported in the literature for similar compatible

thermoplastic overmolded systems. For instance, Perrin et al. reported Mode-I initiation values for Glass-Fiber/Polypropylene (GF/PP) interfaces ranging from approximately 0.6 kJ/m^2 to 2.0 kJ/m^2, depending heavily on cooling rates and fiber architecture [18]. Our results fall well within this established range. While exact numerical alignment is difficult to achieve due to the high sensitivity of diffusion-based bonding to specific injection molding parameters, this comparable magnitude confirms that the BBS method yields realistic fracture data consistent with established adhesion mechanisms. By ensuring a pure Mode-I stress state, this method provides the precise G_{IC} inputs required for calibrating Cohesive Zone Models (CZM) for finite element analysis, offering a distinct advantage over geometry-dependent structural tests.

While the BBS method offers a robust framework for isolating interfacial fracture properties, its application requires specific considerations. The current validation focuses on GF/PP systems. It is acknowledged that different polymer chemistries, such as polyamides or polyesters, significantly influence absolute adhesion and specific fracture mechanisms. However, the mechanical validity of the BBS method, matching the bending stiffness of the arms, remains consistent regardless of the polymer type used. For material pairs with vastly different moduli, careful geometric tuning is required to maintain the stiffness balance. Additionally, the method demands a high degree of experimental precision, particularly regarding specimen tolerances and the use of Digital Image Correlation (DIC), compared to standard mechanical testing. Nevertheless, this increased complexity is a necessary trade-off for data fidelity. By effectively decoupling geometric artifacts from intrinsic bond behavior, the BBS method provides the precise input data required for advanced predictive modeling in industrial applications.

5. Conclusions

This study introduces and validates the Balanced Bending Stiffness (BBS) Method, a novel approach that fundamentally shifts interfacial fracture characterization from post-analytical correction to proactive experimental design. By engineering physically balanced specimens through comparative geometric optimization, the method transforms complex mixed-mode testing into straightforward Mode-I dominant measurements. The BBS method proves practically efficient, converging within a few thickness adjustments across diverse material combinations while utilizing standard testing equipment, making it accessible for both research and industrial applications.

Applying the BBS method in the parametric investigation of fiber-reinforced overmolded systems reveals that mechanical toughening mechanisms play a decisive role in interfacial performance. This finding extends the conventional understanding of adhesion beyond a purely diffusive process, shifting the optimization focus to include the mechanical architecture of the interface. The study demonstrates that fiber content and substrate preheating serve as critical levers for interface optimization, while the superior reinforcement efficiency of long-fiber thermoplastics underscores their high potential for structural overmolding applications.

From an industrial perspective, the BBS Method addresses a critical gap in standardized characterization of overmolded composites, enabling confident material selection and failure prediction in automotive, aerospace, and other safety-critical applications. The method's versatility suggests broader applicability to other asymmetric bimaterial interfaces, positioning it as a foundational tool for hybrid composite characterization. Furthermore, by providing a direct and reliable measurement of the intrinsic Mode-I toughness, the BBS method provides the essential experimental calibration data required for advanced numerical simulations, such as Cohesive Zone Modeling (CZM), enabling more accurate failure prediction at the component level.

This work recommends the BBS Method as both a practical solution to a longstanding measurement challenge and a catalyst for advancing fundamental understanding of interfacial behavior in overmolded hybrid composites. The concept can also be adopted for End-Notched Flexural (ENF) experiments to characterize the Mode-II shear behavior of overmolded materials.

Author Contributions: Conceptualization, A.R.; methodology, A.R.; software, S.N.; validation, S.N., J.M.H.L.; formal analysis, S.N.; investigation, S.N.; resources, J.M.H.L.; data curation, S.N. and R.A.C.L.; writing—original draft preparation, S.N. and A.R.; writing—review and editing, A.T.t.C.; visualization, S.N.; supervision, A.R.; project administration, A.R.; funding acquisition, A.R. and A.T.t.C. All authors have read and agreed to the published version of the manuscript.

Funding: This research received no external funding and fully performed using TNO internal budget.

Institutional Review Board Statement: Not applicable.

Data Availability Statement: The raw data supporting the conclusions of this article will be made available by the authors on request.

Conflicts of Interest: Author Ali Rezaei, Simon Nakze, Jos. M. H Linsen, Rick. A. C Leuven, and A. Tessa ten Cate were employed by the company Brightlands Materials Center, Urmonderbaan 22, 6167 RD Geleen. The remaining declare that the research was conducted in the absence of any commercial or financial relationships that could be construed as a potential conflict of interest.

Abbreviations

ADCB	Asymmetric Double Cantilever Beam
BBS	Balanced Bending Stiffness
CCM	Compliance Calibration Method
CFRP	Continuous Fiber-Reinforced Polymer
CZM	Cohesive Zone Modeling
DIC	Digital Image Correlation
ENF	End-Notched Flexural
GF/PP	Glass Fiber–Reinforced Polypropylene
G_{IC}	Interfacial Fracture Toughness (Mode-I)
LFT	Long-Fiber Thermoplastics
SFT	Short-Fiber Thermoplastics
UD	Unidirectional
IR	Infrared

References

1. Akkerman, R.; Bouwman, M.; Wijskamp, S. Analysis of the Thermoplastic Composite Overmolding Process: Interface Strength. *Front. Mater.* **2020**, *7*, 27. [CrossRef]
2. da Silva, L.F.M.; das Neves, P.J.C.; Adams, R.D.; Spelt, J.K. Analytical models of adhesively bonded joints—Part I: Literature survey. *Int. J. Adhes. Adhes.* **2009**, *29*, 319–330. [CrossRef]
3. Carlsson, L.A.; Adams, D.F.; Pipes, R.B. *Experimental Characterization of Advanced Composite Materials*, 4th ed.; CRC Press: Boca Raton, FL, USA, 2014.
4. Suo, Z.; Hutchinson, J.W. Interface crack between two elastic layers. *Int. J. Fract.* **1990**, *43*, 1–18. [CrossRef]
5. Ziaee, S.; Kerr-Anderson, E.; Johnson, A.; Eastep, D.; Abdel-Magid, B. Effect of high fiber content on properties and performance of CFRTP composites. *J. Compos. Sci.* **2024**, *8*, 364. [CrossRef]
6. Jiang, L.; Zhou, Y.; Jin, F.; Hou, Z. Influence of polymer matrices on the tensile and impact properties of long fiber-reinforced thermoplastic composites. *Polymers* **2023**, *15*, 408. [CrossRef] [PubMed]
7. Miao, T.; Wang, W.; Zhai, Z.; Ding, Y. Effect of injection overmolding parameters on the interface bonding strength of hybrid thermoset–thermoplastic composites. *Polymers* **2023**, *15*, 2879. [CrossRef] [PubMed]
8. Yan, B.; Wu, H.; Jiang, G.; Guo, S.; Huang, J. Interfacial Crystalline Structures in Injection Over-Molded Polypropylene and Bond Strength. *ACS Appl. Mater. Interfaces* **2010**, *2*, 3023–3036. [CrossRef] [PubMed]

9. Heitkamp, T.; Girnth, S.; Kuschmitz, S.; Waldt, N.; Klawitter, G.; Vietor, T. Experimental and numerical investigation of the mechanical properties of 3D-printed hybrid and non-hybrid composites. *Polymers* **2023**, *15*, 1164. [CrossRef] [PubMed]
10. Joppich, T.; Menrath, A.; Henning, F. Advanced Molds and Methods for the Fundamental Analysis of Process Induced Interface Bonding Properties of Hybrid, Thermoplastic Composites. *Procedia CIRP* **2017**, *66*, 137–142. [CrossRef]
11. He, M.Y.; Hutchinson, J.W. Crack deflection at an interface between dissimilar elastic materials. *Int. J. Solids Struct.* **1989**, *25*, 1053–1067. [CrossRef]
12. Réthoré, J.; Gravouil, A.; Morestin, F.; Combescure, A. Estimation of mixed-mode stress intensity factors using digital image correlation and an interaction integral. *Int. J. Fract.* **2005**, *132*, 65–79. [CrossRef]
13. Tvergaard, V.; Hutchinson, J.W. The relation between crack growth resistance and fracture process parameters in elastic–plastic solids. *J. Mech. Phys. Solids* **1992**, *40*, 1377–1397. [CrossRef]
14. Turon, A.; Camanho, P.P.; Costa, J.; Dávila, C.G. A damage model for the simulation of delamination in advanced composites under variable-mode loading. *Mech. Mater.* **2006**, *38*, 1072–1089. [CrossRef]
15. Williams, M.L. The stresses around a fault or crack in dissimilar media. *Bull. Seismol. Soc. Am.* **1959**, *49*, 199–204. [CrossRef]
16. Rice, J.R. Elastic fracture mechanics concepts for interfacial cracks. *J. Appl. Mech.* **1988**, *55*, 98–103. [CrossRef]
17. *ASTM D5528-13*; Standard Test Method for Mode-I Interlaminar Fracture Toughness of Unidirectional Fiber-Reinforced Polymer Matrix Composites. ASTM International: West Conshohocken, PA, USA, 2013.
18. Perrin, F.; Bureau, M.N.; Denault, J.; Dickson, J.I. Mode I interlaminar crack propagation in continuous glass fiber/polypropylene composites: Temperature and molding condition dependence. *Compos. Sci. Technol.* **2003**, *63*, 597–607. [CrossRef]